ACS OMEGA

http://pubs.acs.org/journal/acsodf

Article

Water/InP(001) from Density Functional Theory

Isaac Azahel Ruiz Alvarado* and Wolf Gero Schmidt

Cite This: *ACS Omega* 2022, 7, 19355−19364

Read Online

ACCESS | Metrics & More | Article Recommendations

ABSTRACT: The interface between water and the In-rich InP(001) surface is studied by density functional theory with water coverage ranging from single molecules to multiple overlayers. Single molecules attach preferably to three-fold coordinated surface In atoms. Water dissociation is energetically favorable but hindered by an energy barrier that decreases with increasing water coverage. There is an attractive interaction between InP adsorbed water molecules that leads to the formation of molecular clusters and complete water films for water-rich preparation conditions. Water films on InP are stabilized by anchoring to surface-bonded hydroxyl groups. With increasing thickness, the water films resemble the structural properties of ice Ih. The oxygen and hydrogen evolution reactions on InP are characterized by overpotentials of the order of 1.7−1.8 and 0.2−0.3 eV, respectively. While the calculated bulk positions of the InP band edges are outside the range of the redox potentials for oxygen and hydrogen evolution within local DFT, the situation is different at the actual interface: Here, the interface dipole lifts the InP valence band maximum above the redox potential for oxygen evolution and favors hydrogen evolution.

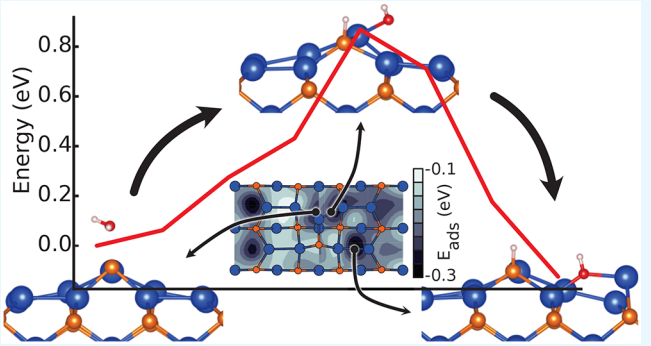

INTRODUCTION

The applications of III−V compound semiconductors range from the area of nanotechnology, where they are used for quantum wells,[1] quantum dots,[2] and nanowires[3] to optoelectronics, multilayered high-efficiency solar cells,[4] and artificial leaves for solar-to-hydrogen conversion.[5] Group-III phosphides show promising results for solar powered water splitting, due to high solar to energy conversion. In particular, the combination of InP with other materials is efficiently used in this context.[6−9] The rapid InP corrosion under operating conditions is one of the problems that still needs to be solved, however.

While the clean InP surface reconstructions are well understood,[10−13] relatively little is known about the microscopic structure and electronic properties of InP in contact with oxygen and water.[14−17] May and co-workers interpret their optical spectroscopy data[18] in terms of a dissociative adsorption of water on InP(001), resulting in the formation of In−O−P bonds. No hydroxyl signatures were found by photoelectron spectroscopy, indicating that the dissociative adsorption of water releases both hydrogen atoms of the water molecule. On the other hand, a computational study by Wood et al.[19] finds the dissociative adsorption of water favorable for GaP surfaces but not for InP. For both substrates, a dissociation barrier of about 0.8 eV was calculated. Photoelectron spectroscopy measurements also detected a dissociative adsorption of water on Ga-rich GaAs(001) surfaces, leading to surface adsorbed OH and H species.[20] Further deprotonation results in the formation of Ga−O, Ga−OH, and As−H bonds. High water pressures cause water physisorption directly on the GaAs surface or to be anchored to Ga−OH bonds. In case of GaP, it was noted that the water surface interaction depends on the surface reconstruction. Ga-rich surfaces show a higher reactivity than P-rich surfaces. Photoelectron and optical spectroscopy[16] suggest the presence of both water and hydroxyl groups on Ga-rich GaP surfaces. This is backed by a theoretical study on the reaction pathways.[21]

The present study aims at a thorough understanding of the interaction between water and the In-rich InP(001) surface. The adsorption and surface reactions of single water molecules, water monolayers, and water multilayers are studied by density functional theory (DFT) calculations. In addition, we explore pathways for oxygen and hydrogen evolution reactions (OER and HER).

Received: February 16, 2022
Accepted: May 6, 2022
Published: June 1, 2022

METHODOLOGY

The present DFT calculations are performed with the Vienna Ab Initio Simulation Package (VASP).[22] The electron exchange and correlation interaction are modeled within the generalized gradient approximation (GGA) using the PBE functional.[23] The electron−ion interaction is described by the projector-augmented wave (PAW) scheme.[24,25] An energy cutoff of 500 eV limits the plane-wave basis used to expand the wave functions. The calculations are performed for periodic supercells that contain 12 atomic layers, the adsorbed water, and a vacuum region of about 15 Å. A dipole correction scheme is used to minimize spurious interactions across the vacuum region. The slab bottom In layer is passivated with pseudohydrogen with $Z = 1.25$. Surface periodicities of 2 × 4 (unit cell of the In-rich (001) surface) and 2 × 12 (for better commensurability with thick water overlayers) were used for the water−InP interface calculations. Adsorption energy convergence tests were performed using 4 × 4 surface unit cells. The corresponding surface Brillouin zones were sampled with Γ-centered 6 × 3 × 1, 12 × 2 × 1, and 3 × 3 × 1 k-point meshes, respectively.

All interfaces are structurally relaxed until the forces acting on the atoms are lower than 0.02 eV/Å. Potential energy surface (PES) calculations were performed to determine the most favorable adsorption sites for low coverages. The PES were sampled at 50 equidistant mesh points. At each mesh point, two and nine different starting configurations are probed for hydroxyl group and water molecule adsorption, respectively. In the calculations, the oxygen ion is laterally fixed. Its vertical distance to the surface as well as all other degrees of freedom are not constrained.

The starting geometries for water overlayers that equal or exceed monolayer coverage were derived from both the ice I_h structure as well as randomized water molecule positions. To determine the ground state of the water overlayers, the total-energy minimization is complemented by simulated annealing. To that end we performed ab initio molecular dynamics (MD) calculations in the NVT (canonical) ensemble using a temperature of 400 K to reproduce ambient liquid water. Temperatures were maintained with a Nosé Hoover Thermostat.[26]

The adsorption energy is calculated as

$$E_{ads} = E_{total} - E_{clean} - E_A \tag{1}$$

where E_{total} and E_{clean} are the total energy of the adsorbed system and the clean surface, respectively. In case of water adsorption, E_A corresponds to the total energy of gas-phase water molecules. In case of hydroxyl group and oxygen adsorption, we define E_A as

$$E_{OH} = E_{H_2O} - \frac{1}{2}E_{H_2} \tag{2a}$$

and

$$E_O = E_{H_2O} - E_{H_2} \tag{2b}$$

while hydrogen adsorption is referenced to gas-phase H_2. These definitions allow for direct comparison between dissociative and molecular adsorption energies. Adsorption energies for specific low coverage structures were corrected for the zero-point energies (ZPE).

In order to compare energetically structures that correspond to different water coverages, one needs to consider the grand canonical potential

$$\Omega = F(n) - n\mu_{H_2O} \approx E(n) - n\mu_{H_2O} \tag{3}$$

where $F(n)$ is the total free energy of the surface with n water molecules adsorbed. It is approximated here by the DFT total energy, assuming similar entropy contributions for different adsorption configurations. The chemical potential μ_{H_2O} accounts for the availability of water. Water rich-conditions are defined by the μ_{H_2O} value for bulk water, which we approximate by calculations for the ice I_h phase. In the following, $\Delta\mu_{H_2O}$ refers to the difference of the water chemical from that of ice I_h. Its dependence on temperature and pressure can be calculated in the approximation of a polyatomic ideal gas[27] as

$$\Delta\mu_{H_2O}(p, T) = -k_B T\left[\ln\left(\frac{p\lambda^3}{k_B T}\right) - \ln(Z_{rot}) - \ln(Z_{vib})\right] \tag{4}$$

where k_B is the Boltzmann constant, λ the de Broglie thermal wavelength of the water molecule

$$\lambda = \sqrt{\frac{2\pi\hbar^2}{mk_B T}} \tag{5}$$

m is the mass of the water molecule, and

$$Z_{rot} = \frac{(2k_B T)^{3/2}(\pi I_1 I_2 I_3)^{1/2}}{\sigma\hbar^3} \tag{6}$$

$$Z_{vib} = \prod_\alpha \left[1 - \exp\left(-\frac{\hbar\omega_\alpha}{k_B T}\right)\right]^{-1} \tag{7}$$

are its rotational and vibrational partition functions, respectively. We used experimental values for the moments of inertia I_i and vibrational frequencies ω_α of a water molecule.[28] The geometrical parameter of a water molecule H_2O is given by $\sigma = 2$ (equal-sided triangle).

Surface chemical reactions, in particular oxygen and hydrogen evolution reactions, are characterized in the present work by the Gibbs free energy $G(p,T)$ differences of products and educts. For the calculation of the Gibbs free energy differences, we follow Nørskov et al.[29] and approximate

$$\Delta G = \Delta E_{tot} + \Delta G_U - \Delta G_{pH} \tag{8}$$

where $\Delta G_U = -e{\cdot}U$ and $\Delta G_{pH} = -k_B T \ln(10){\cdot}$pH, account for the reaction energetics dependence on the potential U and the pH value,[30] respectively. For specific low-coverage structures, we accounted additionally for entropic and ZPE corrections. The reaction energy barriers are calculated in the nudged elastic band (NEB) approximation.[31]

RESULTS AND DISCUSSION

In-rich InP(001) surfaces form a (2 × 4) surface reconstruction featuring a single In−P heterodimer in the uppermost atomic layer for a wide range of preparation conditions.[32] This so-called mixed-dimer structure, see Figure 1, is the starting point for the present calculations.

Previous experimental and theoretical studies[18,19] suggested the sites A−D indicated in Figure 1a to be the most favorable

https://doi.org/10.1021/acsomega.2c00948
ACS Omega 2022, 7, 19355−19364

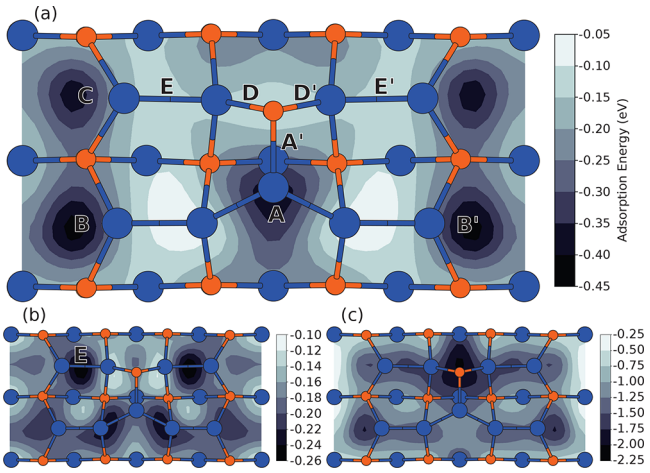

Figure 1. Calculated potential energy surfaces for single water molecules (a), an OH group (b), and a H atom (c) on the InP (001) (2 × 4) mixed-dimer surface. Blue and orange spheres indicate In and P, respectively.

water adsorption positions. Potential energy surface calculations provide a systematic approach to the most favored adsorption geometry for single molecules. The PES calculated here, see Figure 1a, indicates that 3-fold coordinated surface In atoms provide the most favorable bonding sites for water, corresponding to the sites A, B, and C identified already in ref 19. In combination with the PES calculated for the adsorption of OH and H (Figure 1b,c, respectively), the most relevant configurations for the low-coverage stage of the water−InP interface can be identified. The corresponding adsorption energies are listed in Table 1. From convergence tests using 2 × 4 and 4 × 4 surface unit cells, we conclude on an interaction energy of about 5 meV affecting the single molecule adsorption energies. The influence of the electronic entropy at room temperature is about 2 orders of magnitude smaller. Therefore, it is neglected in the following. The ZPE is more important. As seen in Table 1, it typically affects the adsorption energies by about 0.1 eV, in some cases even by 0.22 eV per adsorbate. However, the ZPE does not alter the energy trends derived from the DFT total energies.

Table 1. Adsorption Energies (in eV) and Bond Configurations for H_2O, O, and OH at Specific Sites of the InP Mixed-Dimer Surface, cf. Figure 1

site	configuration	E_{ads} [a]	E_{ads} [a,b]
B	H_2O−In	−0.408	−0.324
A	H_2O−In	−0.384	−0.302
A′	In−O−P	0.387	0.160
D	OH−P	0.665	0.591
A	In−OH	0.646	0.540
E	In−OH−In	−0.073	−0.158
A	In−OH and P−H[c]	−0.274	−0.291
E	In−OH−In and P−H[c]	−0.508	−0.524
B and B′	H_2O−In	−0.989	−0.791
D and D′	In−O−P	−0.175	−0.621
E and E′	In−OH−In	−0.200	−0.369

[a]Positive energies characterize configurations unfavorable with respect to an intact adsorbed water molecule. [b]Includes ZPE corrections. [c]P−H bond forms on In−P mixed dimer.

The most favorable water adsorption configuration at the site B along with the adsorption-induced charge density redistribution is shown in Figure 2. The water molecule donates electrons of its $1b_1$ orbital into the empty In dangling bond of p_z character.[10] This results in a weak O−In bond with length 2.5 Å formed at the surface. The substrate geometry is modified only slightly upon adsorption. No water-induced electronic states appear in the energy region of the InP band gap.

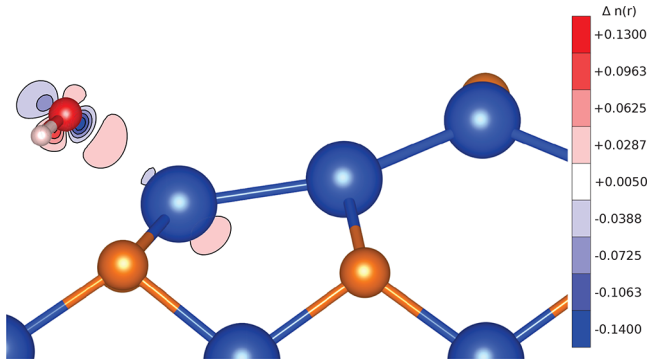

Figure 2. Structural configuration and water-induced charge redistribution for water adsorbed on InP (001) on site B. Red and blue isosurfaces indicate regions of charge accumulation and depletion, respectively.

Experimentally, water adsorption was reported to be dissociative,[18] with oxygen bound near the phosphorus atom of the mixed-dimer (sites D and D′ in Figure 1) while previous theoretical results[19] found molecular adsorption to be favored over dissociation. Here it must be said, however, that in ref 19 the possibility of water dissociation was studied only for adsorption on the mixed-dimer. The present calculations support dissociative adsorption, resulting in a configuration different from the one proposed in ref 18, however. Rather, the hydroxyl group is attached to an In−In bond (site E in Figure 1) and the hydrogen adsorbs at the mixed-dimer P atom, as shown in Figure 3. This configuration is 0.1 eV (0.2 eV with ZPE corrections) lower in energy than the most favorable molecular adsorption at site B. The dissociative adsorption leads to a marked distortion of the InP(001) surface geometry, induced in particular by the insertion of the hydroxyl group oxygen into the second layer In−In bond. As seen by the charge-density redistribution in Figure 3, strong In−O−In and

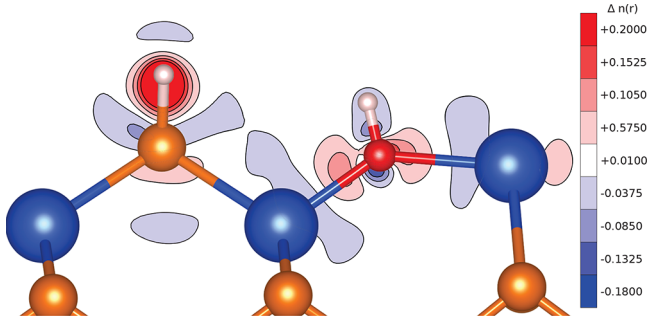

Figure 3. Structural configuration and water-induced charge redistribution for water dissociatively adsorbed on InP (001), with OH on site E and H on the top P. Red and blue isosurfaces indicate regions of charge accumulation and depletion, respectively.

https://doi.org/10.1021/acsomega.2c00948
ACS Omega 2022, 7, 19355−19364

P−H bonds form. Nevertheless, similarly to the intact molecule adsorption, no water-induced electronic states appear in the energy region of the InP band gap.

The energy barrier for water dissociation is calculated here using the nudged elastic band method. Molecular adsorption at site A is assumed to be the starting configuration. Six images at equidistant points between the starting configuration and the dissociatively adsorbed OH group at site E and hydrogen at the topmost P atom are considered. The energy path is shown in Figure 4. The transition state corresponds to the hydroxyl

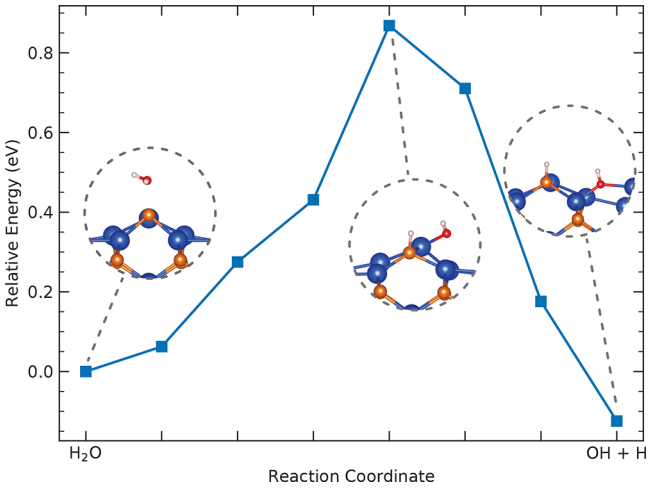

Figure 4. Minimum energy path for dissociative adsorption of single water molecules on InP(001). The starting configuration is the water molecule adsorbed at site A and the final configuration corresponds to the one shown in Figure 3.

group transfer from position A to position E. We obtain an energy barrier of 0.87 eV. This of the same order of magnitude as determined earlier for dissociation on the mixed dimer.[19]

To study a slightly increased water coverage, we consider the adsorption of two molecules per surface unit cell. The minimum energy configuration for molecular adsorption corresponds to the molecules bonded at sites B and B′, cf. Figure 1a. Compared to single molecules adsorbed at these sites, an energy reduction of 0.09 eV (0.07 eV with ZPE corrections) per molecule is found. This demonstrates an attractive interaction and suggests the study of higher water coverages. In the following, we increase the water coverage to up to 56 molecules per (2 × 4) surface unit cell. Given that the influence of the zero-point corrections does not alter the energy trends derived for low-coverage water adsorption, ZPE corrections are neglected for high coverages.

The phase diagram in Figure 5 compares the energetics of various coverages of molecularly adsorbed water. It can be seen that the one-monolayer configuration (Figure 6a) is more favored than small molecular clusters comprising up to five molecules (see inset in Figure 5). Even more favorable, however, is the water bilayer (Figure 6b). According to the present calculations, for intermediate values of the water chemical potential ($\Delta\mu_{H_2O} \approx 0.5$ eV, corresponding roughly to standard pressure at room temperature) there will be a direct transition from the clean InP surface to the water bilayer covered surface. For more water-rich conditions, even thicker water layers will form. For computational reasons, the coverage in the present study is limited to three monolayers (Figure 6c).

Structurally, the one, two and three water layer configurations bear some similarity to ice I_h, see Figure 6. Because of the incommensurability of the ice I_h basal plane with the InP (2 × 4) surface unit cell, as well as due to the InP surface morphology, however, some disorder arises. In particular, irregular pentagons and hexagons form. The mono- and bilayer structures are characterized by water O bonded to three-fold coordinated In atoms, resembling the single molecule bonding to sites A, B, and C in Figure 1. The number of these bonds reduces upon formation of the water bilayer. They are completely quenched for the three-layer structure, which is strongly reminiscent of ice I_h. The InP surface phase diagram in dependence on temperature and water partial pressure is shown in Figure 7. It should be noted that at the transition between the clean InP surface and the water covered substrate some variety of adsorption configurations can be expected: As shown by the inset in Figure 5, in a narrow range of the water chemical potential many competing structures occur, that is, a strong influence of kinetic effects on the actual interface configuration will lead to a variety of interface structures.

A variety of stable dissociated water adsorption configurations can be identified in case of the water-layer covered InP(001) surfaces. The most favorable one for the monolayer covered surface is shown in Figure 8. It corresponds to hydroxyl attached to second layer In−In bonds (bonding site E) and hydrogen attached to the mixed-dimer P atom. This configuration is stable also upon hydrogen transfer from the mixed-dimer to a H_2 reservoir. This contrasts with similar adsorption configurations without the water monolayer, which are not stable upon H desorption. The stability of the dissociated configurations in the presence of the hydrate shell can be explained by the fact that the surface bonded OH group acts as an anchor for the water layer above. Similar findings are reported for the GaAs(100) surfaces.[20] The hydration shell also affects the barrier for water dissociation, as shown the NEB calculations in Figure 9. Here the minimum energy path for a molecule from the water layer that dissociates and adsorbs at the surface is shown. The molecule, originally in a local minimum at the interface between the water layer and the InP surface, needs to overcome a barrier of ∼0.3 eV for dissociation. However, the entire energy path during the dissociation is below the energy of the starting configuration. The hydrate shell also affects the energy barriers involved in the formation of surface adsorbed hydroxyl groups. For example, we calculate a nearly vanishing energy barrier of 7 × 10^{-3} eV for the H_2O−In + In−O−In → OH−In + In−OH−In process. Oxygen bonding close to the topmost P atom, as concluded from experimental data,[18] however, remains unfavorable also for the water layer covered surface.

Finally, we explore the energetics of water splitting. The corresponding redox reaction consists of the oxidation $2H_2O \rightarrow O_2 + 4H^+ + 4e^-$ and the reduction $4H^+ + 4e^- \rightarrow 2H_2$, known as oxygen evolution reaction (OER) and hydrogen evolution reaction (HER), respectively. They are studied here by calculating the Gibbs free energy $G(p,T)$ changes according to eq 8. We assume the reaction $H_2 \rightleftharpoons 2(H^+ + e^-)$ to be in equilibrium, that is, the reference potential is given by the "numerical" hydrogen electrode, corresponding to a vanishing Gibbs free energy difference $\Delta G = 0$. Consequently, the energy of proton−electron pairs in the reaction pathways is given by $E(H^+ + e^-) = \frac{1}{2}E_{H_2}$. The overpotential η is defined as the difference between the largest energy difference ΔG and the

https://doi.org/10.1021/acsomega.2c00948
ACS Omega 2022, 7, 19355−19364

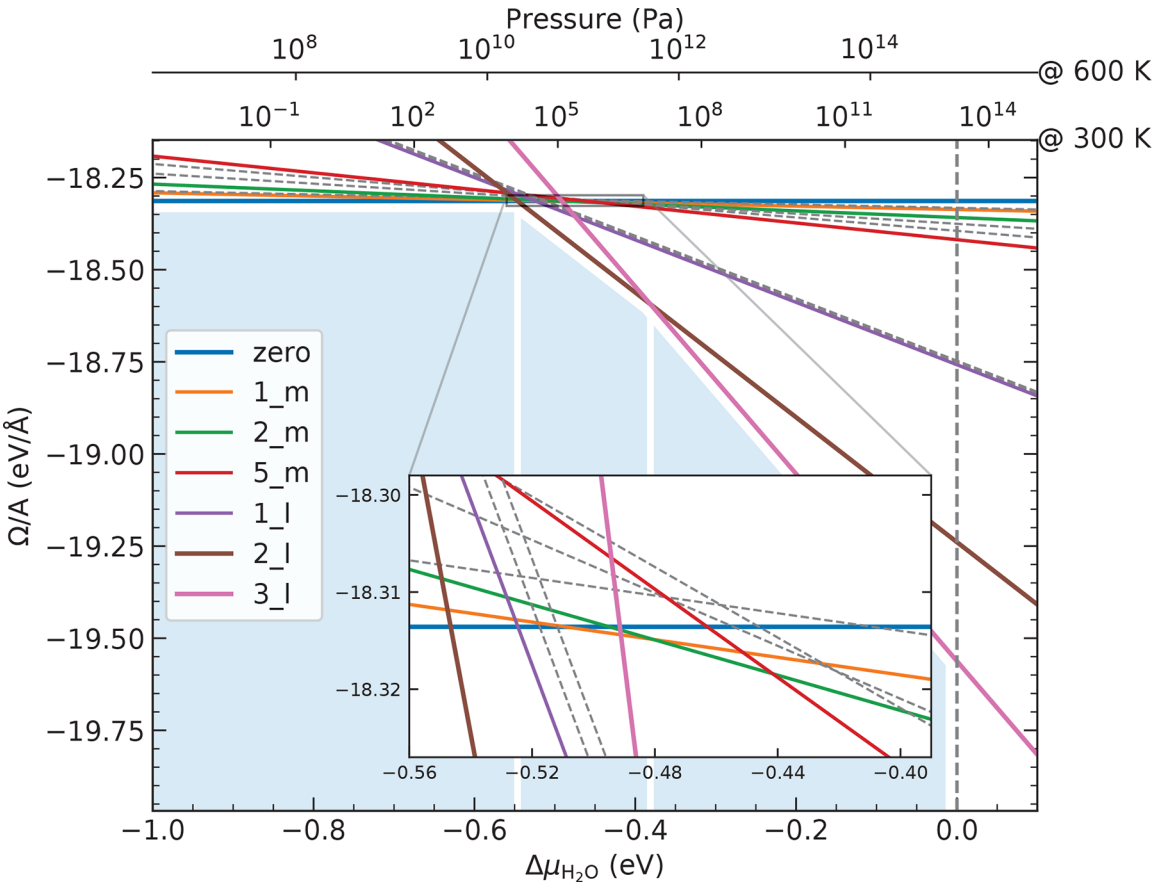

Figure 5. Phase diagram of the water-adsorbed InP(001) surface in dependence on the water chemical potential $\Delta\mu_{H_2O}$. Here adsorption configurations comprising 1, 2, and 5 molecules (m) are compared with the formation of 1, 2, and 3 layers (l) and the clean surface (zero). The pressure and temperature dependence of $\Delta\mu_{H_2O}$ refer to eq 4.

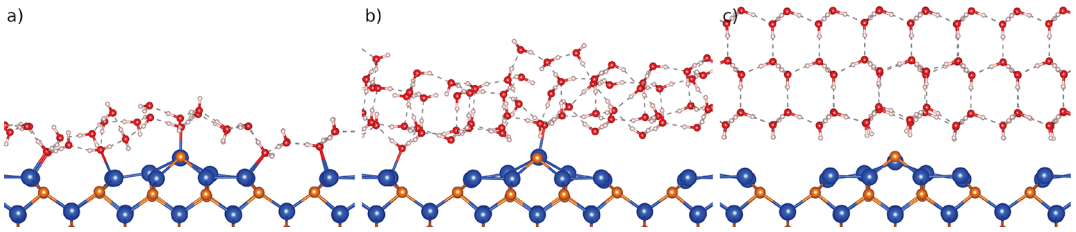

Figure 6. Energetically favorable In−P (001)(2 × 4) structures with one (a), two (b), and three (c) adsorbed water layers.

corresponding potential at zero pH. The water to oxygen oxidation potential for the OER is 1.23 eV[33] while that for HER vanishes by definition.

The are many possible pathways for the OER. Here, we restrict ourselves to the associative reaction mechanism for water splitting.[29,34] This mechanism is assumed to have a peroxide intermediate OOH adsorbed on the surface. An alternative mechanism would be for two water molecules to separately dissociate into two surface-bonded O atoms. The activation barrier associated for the recombination of two adjacent oxygen atoms into O_2 is rather large.[35] Here we calculate an energy barrier of ∼4 eV for the recombination process within the NEB method, rendering this process less likely. The steps of the associative chemical reactions read

$$H_2O^* \rightarrow OH^* + H^+ + e^- \quad (A)$$

$$OH^* \rightarrow O^* + H^+ + e^- \quad (B)$$

$$H_2O + O^* \rightarrow OOH^* + H^+ + e^- \quad (C)$$

$$OOH^* \rightarrow O_2^* + H^+ + e^- \quad (D)$$

where X* denotes a species X adsorbed at the surface. The present calculations of the respective reaction energetics are based on the most favored adsorption configurations determined from the potential energy surfaces discussed above. On the basis of the respective energy differences, the data in Figure 10 are obtained. Here, results neglecting and including ZPE corrections are compared. The reaction A is exergonic for neutral conditions, and there is only a very small energy increase observed for reaction B. With ZPE corrections both reactions, A and B, are exergonic. This could possibly explain the experimental findings in ref 18, where no persistent hydroxyl groups, but the release of gaseous hydrogen, were observed. There is a considerable energy required for reaction C, necessitating an external bias voltage. Applying an external

https://doi.org/10.1021/acsomega.2c00948
ACS Omega 2022, 7, 19355−19364

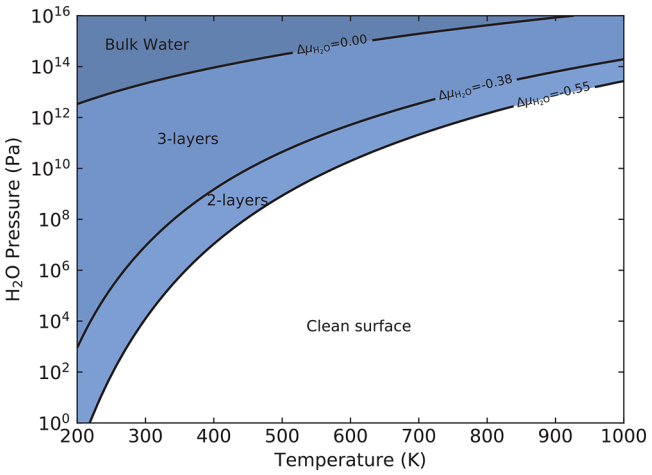

Figure 7. Phases diagram of the InP (001) mixed dimer surface as a function of the temperature and pressure. The values of the water chemical potential μ_{H_2O} for which the phase transitions occur are marked by the solid lines.

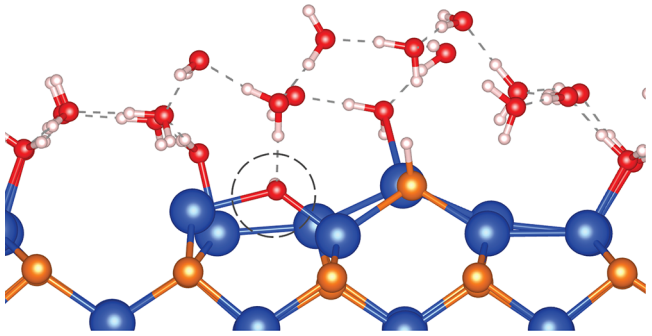

Figure 8. Most stable water dissociation configuration identified here for the monolayer covered InP (001) surface. The surface adsorbed OH group is highlighted.

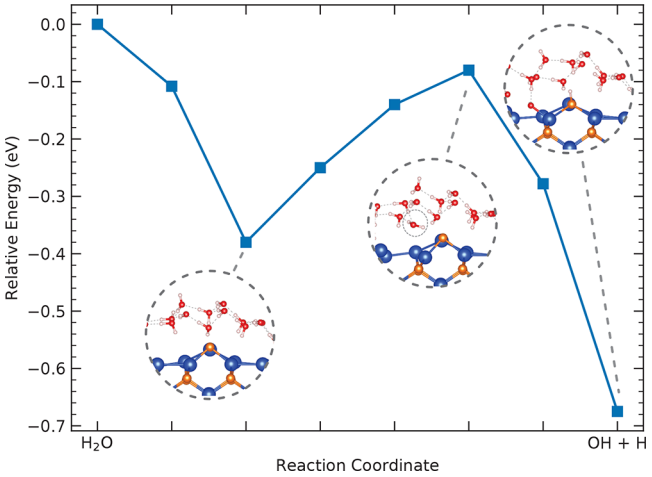

Figure 9. Minimum energy path for dissociative adsorption of single water molecules embedded at the water−InP interface.

potential of 3 eV results in the orange solid curve shown in Figure 10. Generally, we find that the inclusion of ZPE corrections tends to reduce the OER energy differences. Fortuitously, however, the change in the overpotential due to ZPE corrections is small. We calculate an overpotential η of about 1.7 eV. The reactions depend on the acidity of the

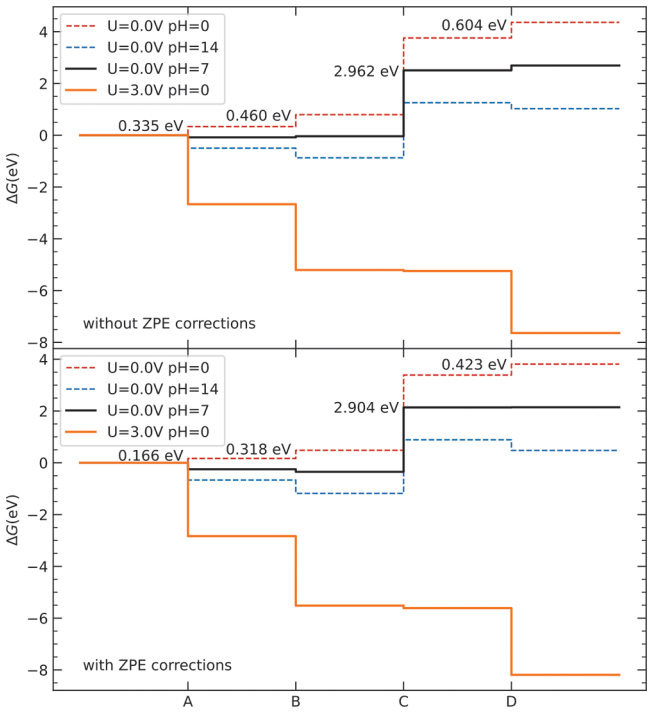

Figure 10. Comparison of the Gibbs free energy for the OER for different potentials and pH values. Bottom and top figures with and without ZPE energy term, respectively. Numbers represent the energy barriers for 0 pH and no potential.

electrolyte. Decreasing pH, that is, increasing acidity favors H-adsorbed surfaces and requires larger potentials for hydrogen desorption. Reaction A becomes endergonic for pH lower than 5.5 (2.8 with ZPE corrections). At zero pH, the energy difference amounts to 0.33 eV, and around half of that with ZPE corrections, 0.17 eV. Reaction B becomes exergonic for pH larger than 7.8 (5.3 with ZPE corrections), allowing a water molecule to release surface adsorbed oxygen without an external potential. The reaction energies for extreme acidic and alkaline electrolytes are shown by dashed lines in Figure 10. It should be kept in mind, however, that the reactions itself will modify the pH value and that for alkaline conditions different OER processes might occur.[30,36]

The HER process involves the reduction of the protons to molecular hydrogen and is modeled here as

$$* + H^+ + e^- \rightarrow H^* \quad \text{(E)}$$

$$H^* + H^+ + e^- \rightarrow H_2^* \quad \text{(F)}$$

where we employ the mixed dimer as most favored adsorption site for both atomic and molecular hydrogen. The corresponding Gibbs free energy differences are shown in Figure 11. A potential of 0.68 and 0.6 eV is required for reaction E in neutral electrolytes with and without ZPE corrections, respectively, as shown by the black solid curve. Increasing the pH increases this value, as less hydrogen ions are available for surface adsorption. In contrast, the energy required for both reactions E and F is lowered for acidic conditions. At pH levels below 3.6 reaction F is exergonic, that is, occurs spontaneously. At extreme acidic conditions, corresponding to zero pH, the energy difference for reaction E is 0.19 eV (0.26 eV with ZPE corrections), which also defines the overpotential, see dashed line in Figure 11. The ZPE corrections increase the energy required for the reaction E, in contrast to the reduction of the

https://doi.org/10.1021/acsomega.2c00948
ACS Omega 2022, 7, 19355−19364

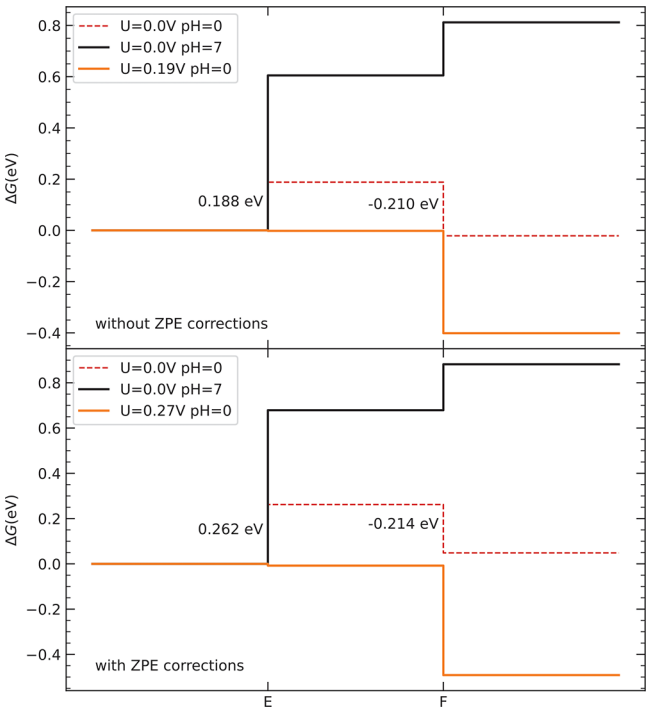

Figure 11. Comparison of the Gibbs free energy for the HER for different potentials and pH values. Bottom and top figures with and without ZPE energy term, respectively. Numbers represent the energy barriers for 0 pH and no potential.

OER energies and in contrast to reaction F. Even if ZPE corrections slightly (by less than 0.1 eV) increase the HER overpotential, it is still about an order of magnitude lower than that for the OER. In addition to the favorable reaction energetics found here, the possibility of long-range surface hydrogen transport at the InP(001)−water interface pointed out in ref 37 may enhance hydrogen evolution on the InP surface.

However, the OER and HER energetics discussed so far is limited to the thermodynamics and does not consider the kinetics of the underlying processes. The latter are determined by the reaction barriers. In the reaction A, for example, the dissociation of a water molecule into a surface adsorbed hydroxyl group and a desorbing proton occurs. For the dissociation of surface adsorbed water into surface adsorbed OH and H on clean InP an energy barrier of about 0.8 eV needs to be overcome, see Figure 4. In addition, there could be an additional kinetic barrier for hydrogen desorption. Using the NEB method and assuming desorption from the adsorbed water molecule configuration, we calculate that an energy of about 2.7 eV is required for hydrogen desorption, see Figure 12. This energy matches in fact the difference in the chemical potentials of molecular and atomic hydrogen complemented by the Gibbs free energy difference of reaction A. Thus, as one might expect, the water dissociation rather than the hydrogen desorption presents an additional barrier hindering the OER.

Such barriers, however, can be expected to be modified by the presence of additional water molecules forming a hydration shell. In Figure 13, we show the OER energetics assuming the reactions to take place in the presence of one monolayer water adsorbed. The energies shown in Figure 13 correspond to the average of the six most favorable water overlayer configurations. Because the large number of molecules involved, ZPE

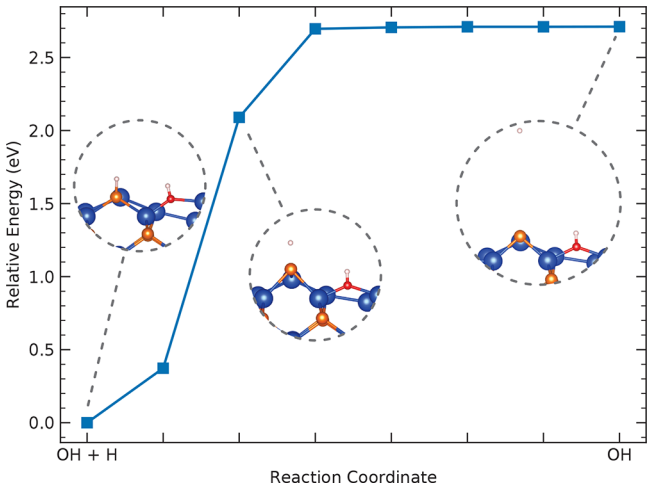

Figure 12. Minimum energy paths of the desorption of a hydrogen on the surface. The starting point is the OH adsorbed at site E and H on the top P, corresponding to the final configuration of the water dissociation shown in Figure 4.

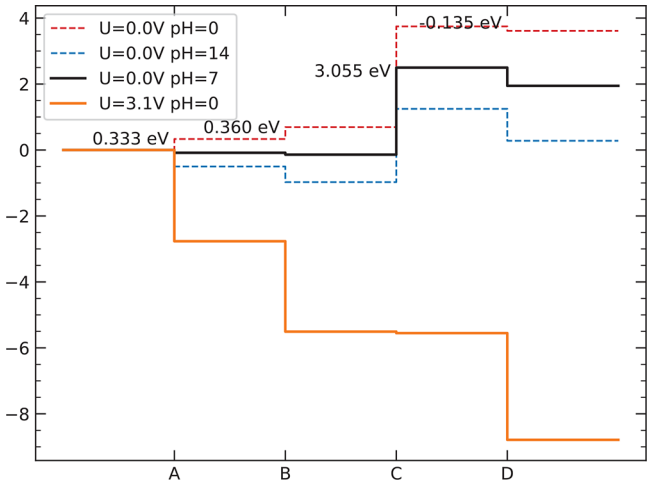

Figure 13. Comparison of the Gibbs free energy for the OER in the presence of one water monolayer for different potentials and pH values. Numbers represent the energy barriers for 0 pH and no potential.

corrections were neglected. It can be seen that reactions B and D are the ones most affected by the hydration shell. They become favorable. Reaction C, on the other hand, requires slightly more energy, resulting in an increase of the overpotential to η = 1.83 eV. The HER energetics in the presence of a water monolayer is shown in Figure 14. Reaction E is hindered by the additional water layer. This results in an increase in the overpotential to η = 0.31 eV. Thus, the overpotentials for both OER and HER are slightly increased by the presence of additional water. We cannot exclude, however, that reaction mechanisms different from the ones consider here may change this picture.

The absolute energy positions of valence and conduction bands are crucial for water splitting: The conduction band minimum should be above the redox potential for hydrogen evolution, and the valence band maximum needs to be below the redox potential for oxygen evolution. Figure 15 compares the band alignments of InP with the water oxidation and hydrogen reduction potentials, 1.23 and 0.00 eV, respectively.

https://doi.org/10.1021/acsomega.2c00948
ACS Omega 2022, 7, 19355−19364

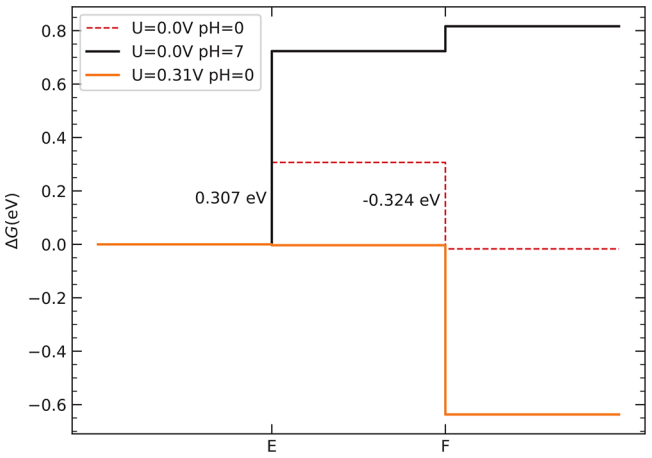

Figure 14. Comparison of the Gibbs free energy for the HER in the presence of one water monolayer for different potentials and pH values. Numbers represent the energy barriers for 0 pH and no potential.

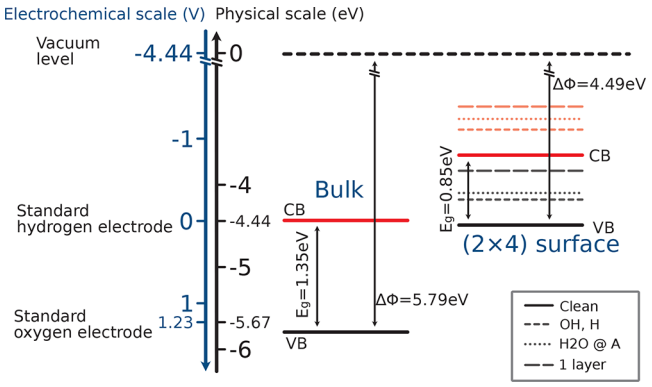

Figure 15. Band alignment of InP bulk and surface (calculated on the DFT-GGA level of theory) in relation to the water splitting redox potentials. Red/black lines depict CBs/VBs.

On the physical scale, they correspond to −5.67 and −4.44 eV. To locate the InP band edges we calculate the work function ΔΦ, that is, the energy necessary to transfer an electron from the valence band to the vacuum level, and assume a band gap of 1.35 eV for the bulk. Our calculations for InP bulk result in ΔΦ = 5.79. This leads to OER and HER potentials that are both inside the band gap, albeit close to the edges, in agreement with the data reported in ref 38. This would suggest InP as a candidate for unbiased water splitting. However, the electronic structure obtained on the DFT-GGA level of energy suffers from an inaccurate description of the electron exchange and correlation effects. In order assess the influence of the GGA on the energy alignment, hybrid DFT calculations using the HSE functional[39] were performed. They increase the work function to ΔΦ = 6.01, which seems to indicate that InP is suitable for OER rather than HER. However, this is still not the complete picture. The bulk calculations do not necessarily describe the electron energies at the surface correctly. They may be affected by an electric dipole layer arising from surface relaxation and reconstruction. In addition, surface states and adsorbates can be expected to modify the work function. In case of Ga-rich GaP surfaces, a work function reduction upon water adsorption was assumed as a result of a dipole layer formed by water molecules that bond with hydrogen in down position.[40] Depending on the surface polarity, a work function increase or decrease was found upon water adsorption on lithium niobate.[41] In case of InP(001) it was found earlier that the work function decreases gradually with increasing In coverage.[10] Here a work function of ΔΦ = 4.49 and a band gap of 0.85 eV are calculated for the mixed-dimer InP(001)(2 × 4) surface on the DFT-GGA level of theory. This lifts the valence band edge above the oxidation potential, see Figure 15. This result is corroborated by hybrid DFT. It predicts a work function of ΔΦ = 4.75 and a band gap of 1.46 eV for the mixed-dimer reconstructed surface. The adsorption of hydrogen and hydroxyl groups, single water molecules as well as water monolayer formation reduces the work function further, below the value of the clean InP surface. Thus, the present calculations suggest the InP surface primarily for hydrogen evolution.

CONCLUSIONS

In summary, we studied the interaction of water with In-rich InP(001) surfaces using density functional theory. Zero-point energy corrections are found to influence molecular adsorption energies by up to 0.2 eV as well as to slightly modify the OER and HER energetics.

Single adsorbed water molecules are found to bond preferentially to three-fold coordinated In surface atoms. Dissociative adsorption is found to be more favorable than molecular adsorption but hindered by a sizable energy barrier. Upon dissociation, the hydroxyl group preferentially bonds to In−In dimers, while hydrogen adsorbs at the mixed-dimer P atom.

Upon increasing the water coverage, an attractive interaction between the water molecules governs the interface morphology. There is a small range of preparation conditions corresponding to intermediate values of the water chemical potential where a variety of structures are nearly degenerate, and single molecules, molecular clusters, and completely water-covered surface patches coexist. For water-rich conditions, water layers form. This leads to a distinct reduction of the reaction barrier for water dissociation and may explain experimental findings stating dissociative adsorption.

While the morphology of the monolayer water film is strongly influence by the InP surface structure and characterized by numerous surface In−water oxygen bonds, multilayer structures resemble the molecular arrangement in ice I_h. Surface-bonded hydroxyl groups formed upon dissociation of water act as anchor points for the water overlayer, similar to observations for other III−V materials.

The overpotentials for OER and HER are calculated here to be of the order of 1.7−1.8 and 0.2−0.3 eV, respectively. These values can be lowered upon variation of the electrolyte pH. While DFT calculations of bulk InP suggest the material for unbiased water splitting, the picture changes if InP surface calculations are performed. They lift the valence-band maximum above the oxidation potential. This finding is corroborated by hybrid DFT. Both the calculated overpotentials as well as the energy position of the InP band edges thus suggest InP surfaces for hydrogen evolution. The HER may be additionally assisted by In−O−In bonds that result from InP surface oxidation and provide additional hydrogen adsorption sites.

https://doi.org/10.1021/acsomega.2c00948
ACS Omega 2022, 7, 19355−19364

AUTHOR INFORMATION

Corresponding Author

Isaac Azahel Ruiz Alvarado − *Lehrstuhl für Theoretische Materialphysik, Universität Paderborn, 33095 Paderborn, Germany;* orcid.org/0000-0002-4710-1170; Email: azahel@mail.upb.de

Author

Wolf Gero Schmidt − *Lehrstuhl für Theoretische Materialphysik, Universität Paderborn, 33095 Paderborn, Germany;* orcid.org/0000-0002-2717-5076

Complete contact information is available at: https://pubs.acs.org/10.1021/acsomega.2c00948

Notes

The authors declare no competing financial interest.

ACKNOWLEDGMENTS

Financial support by DFG (PAK981, SCHM1361/26) is gratefully acknowledged. The authors thank the Paderborn Center for Parallel Computing (PC^2) and the Höchstleistungs-Rechenzentrum Stuttgart (HLRS) for grants of high-performance computer time.

REFERENCES

(1) Wang, Q.; Wang, H.; Zhang, B.; Wang, X.; Liu, W.; Wang, J.; Wang, J.; Fan, J.; Zou, Y.; Ma, X. Integrated fabrication of a high strain InGaAs/GaAs quantum well structure under variable temperature and improvement of properties using MOCVD technology. *Opt. Mater. Express* **2021**, *11*, 2378−2388.

(2) Zhao, T.; Oh, N.; Jishkariani, D.; Zhang, M.; Wang, H.; Li, N.; Lee, J. D.; Zeng, C.; Muduli, M.; Choi, H.-J.; Su, D.; Murray, C. B.; Kagan, C. R. General Synthetic Route to High-Quality Colloidal III-V Semiconductor Quantum Dots Based on Pnictogen Chlorides. *J. Am. Chem. Soc.* **2019**, *141*, 15145−15152.

(3) Barrigón, E.; Heurlin, M.; Bi, Z.; Monemar, B.; Samuelson, L. Synthesis and Applications of III-V Nanowires. *Chem. Rev.* **2019**, *119*, 9170−9220.

(4) Geisz, J. F.; France, R. M.; Schulte, K. L.; Steiner, M. A.; Norman, A. G.; Guthrey, H. L.; Young, M. R.; Song, T.; Moriarty, T. Six-junction III-V solar cells with 47.1% conversion efficiency under 143 Suns concentration. *Nat. Energy* **2020**, *5*, 326−335.

(5) May, M. M.; Lewerenz, H. J.; Lackner, D.; Dimroth, F.; Hannappel, T. Efficient direct solar-to-hydrogen conversion by in situ interface transformation of a tandem structure. *Nat. Commun.* **2015**, *6*, 8286.

(6) Heller, A.; Vadimsky, R. G. Efficient Solar to Chemical Conversion: 12 Efficient Photoassisted Electrolysis in the [p-type InP(Ru)]/HCl-KCl/Pt(Rh) Cell. *Phys. Rev. Lett.* **1981**, *46*, 1153−1156.

(7) Niu, M.; Cao, D.; Sui, K.; Liu, C. InP/TiO_2 heterojunction for photoelectrochemical water splitting under visible-light. *Int. J. Hydrogen Energy* **2020**, *45*, 11615−11624.

(8) Dong, J.; Zhang, X.; Lu, G.; Wang, C. Generation of enhanced stability of SnO/$In(OH)_3$/InP for photocatalytic water splitting by SnO protection layer. *Front. Energy* **2021**, *15*, 710−720.

(9) Lee, M. H.; Takei, K.; Zhang, J.; Kapadia, R.; Zheng, M.; Chen, Y.-Z.; Nah, J.; Matthews, T. S.; Chueh, Y.-L.; Ager, J. W.; Javey, A. p-Type InP Nanopillar Photocathodes for Efficient Solar-Driven Hydrogen Production. *Angew. Chem., Int. Ed.* **2012**, *51*, 10760−10764.

(10) Schmidt, W.; Bechstedt, F. Geometry and electronic structure of InP(001)(2 × 4) reconstructions. *Surf. Sci.* **1998**, *409*, 474−484.

(11) Hahn, P. H.; Schmidt, W. G. Surface Ordering of P-rich InP(001): Hydrogen Stabilization vs Electron Correlation. *Surf. Rev. Lett.* **2003**, *10*, 163−167.

(12) Schmidt, W. G.; Hahn, P. H.; Bechstedt, F.; Esser, N.; Vogt, P.; Wange, A.; Richter, W. InP(001)-(2 × 1) Surface: A Hydrogen Stabilized Structure. *Phys. Rev. Lett.* **2003**, *90*, 126101.

(13) Li, C. H.; Sun, Y.; Law, D. C.; Visbeck, S. B.; Hicks, R. F. Reconstructions of the InP(111)A surface. *Phys. Rev. B* **2003**, *68*, 085320.

(14) Chen, G.; Visbeck, S. B.; Law, D. C.; Hicks, R. F. Structure-sensitive oxidation of the indium phosphide (001) surface. *J. Appl. Phys.* **2002**, *91*, 9362−9367.

(15) Santosh, K. C.; Wang, W.; Dong, H.; Xiong, K.; Longo, R. C.; Wallace, R. M.; Cho, K. First principles study on InP (001)-(2 × 4) surface oxidation. *J. Appl. Phys.* **2013**, *113*, 103705−8.

(16) May, M. M.; Supplie, O.; Hóhn, C.; Zabka, W.-D.; Lewerenz, H.-J.; van de Krol, R.; Hannappel, T. Water-induced modifications of GaP(100) and InP(100) surfaces studied by photoelectron spectroscopy and reflection anisotropy spectroscopy. *Solar Hydrogen and Nanotechnology VIII* **2013**, 46−52.

(17) Henrion, O.; Klein, A.; Jaegermann, W. Water adsorption on UHV cleaved InP(110) surfaces. *Surf. Sci.* **2000**, *457*, L337−L341.

(18) May, M. M.; Lewerenz, H.-J.; Hannappel, T. Optical in Situ Study of InP(100) Surface Chemistry: Dissociative Adsorption of Water and Oxygen. *J. Phys. Chem. C* **2014**, *118*, 19032−19041.

(19) Wood, B. C.; Schwegler, E.; Choi, W. I.; Ogitsu, T. Surface Chemistry of GaP(001) and InP(001) in Contact with Water. *J. Phys. Chem. C* **2014**, *118*, 1062−1070.

(20) Zhang, X.; Ptasinska, S. Dissociative Adsorption of Water on an H_2O/GaAs(100) Interface: In Situ Near-Ambient Pressure XPS Studies. *J. Phys. Chem. C* **2014**, *118*, 4259−4266.

(21) Jeon, S.; Kim, H.; Goddard, W. A.; Atwater, H. A. DFT Study of Water Adsorption and Decomposition on a Ga-Rich GaP(001)(2 × 4) Surface. *J. Phys. Chem. C* **2012**, *116*, 17604−17612.

(22) Kresse, G.; Furthmüller, J. Efficiency of ab-initio total energy calculations for metals and semiconductors using a plane-wave basis set. *Comput. Mater. Sci.* **1996**, *6*, 15−50.

(23) Perdew, J. P.; Burke, K.; Ernzerhof, M. Generalized Gradient Approximation Made Simple. *Phys. Rev. Lett.* **1996**, *77*, 3865−3868.

(24) Blöchl, P. E. Projector augmented-wave method. *Phys. Rev. B* **1994**, *50*, 17953−17979.

(25) Kresse, G.; Joubert, D. From ultrasoft pseudopotentials to the projector augmented-wave method. *Phys. Rev. B* **1999**, *59*, 1758−1775.

(26) Nosé, S. A unified formulation of the constant temperature molecular dynamics methods. *J. Chem. Phys.* **1984**, *81*, 511−519.

(27) Landau, L.; Lifshitz, E. *Statistical Physics, Part I*; Butter-Heiemann: Oxford, 1981.

(28) Laurie, V. W.; Herschbach, D. R. Influence of Vibrations on Molecular Structure Determinations. II. Average Structures Derived from Spectroscopic Data. *J. Chem. Phys.* **1962**, *37*, 1687−1693.

(29) Nørskov, J. K.; Rossmeisl, J.; Logadottir, A.; Lindqvist, L.; Kitchin, J. R.; Bligaard, T.; Jónsson, H. Origin of the Overpotential for Oxygen Reduction at a Fuel-Cell Cathode. *J. Phys. Chem. B* **2004**, *108*, 17886−17892.

(30) Liang, Q.; Brocks, G.; Bieberle-Hütter, A. Oxygen evolution reaction (OER) mechanism under alkaline and acidic conditions. *Journal of Physics: Energy* **2021**, *3*, 026001.

(31) Henkelman, G.; Uberuaga, B. P.; Jónsson, H. A climbing image nudged elastic band method for finding saddle points and minimum energy paths. *J. Chem. Phys.* **2000**, *113*, 9901−9904.

(32) Schmidt, W. G.; Bechstedt, F.; Esser, N.; Pristovsek, M.; Schultz, C.; Richter, W. Atomic structure of InP(001)-(2 × 4): A dimer reconstruction. *Phys. Rev. B* **1998**, *57*, 14596−14599.

(33) Srinivasu, K.; Ghosh, S. K. Photocatalytic splitting of water on s-triazine based graphitic carbon nitride: an ab initio investigation. *J. Mater. Chem. A* **2015**, *3*, 23011−23016.

(34) Rossmeisl, J.; Logadottir, A.; Nørskov, J. Electrolysis of water on (oxidized) metal surfaces. *Chem. Phys.* **2005**, *319*, 178−184.

(35) Nørskov, J.; Bligaard, T.; Logadottir, A.; Bahn, S.; Hansen, L.; Bollinger, M.; Bengaard, H.; Hammer, B.; Sljivancanin, Z.; Mavrikakis,

M.; Xu, Y.; Dahl, S.; Jacobsen, C. Universality in Heterogeneous Catalysis. *J. Catal.* **2002**, *209*, 275−278.
(36) Birss, V. I.; Damjanovic, A. Oxygen Evolution at Platinum Electrodes in Alkaline Solutions: I. Dependence on Solution pH and Oxide Film Thickness. *J. Electrochem. Soc.* **1987**, *134*, 113−117.
(37) Wood, B. C.; Schwegler, E.; Choi, W. I.; Ogitsu, T. Hydrogen-Bond Dynamics of Water at the Interface with InP/GaP(001) and the Implications for Photoelectrochemistry. *J. Am. Chem. Soc.* **2013**, *135*, 15774−15783.
(38) Vurgaftman, I.; Meyer, J. R.; Ram-Mohan, L. R. Band parameters for III-V compound semiconductors and their alloys. *J. Appl. Phys.* **2001**, *89*, 5815−5875.
(39) Krukau, A. V.; Vydrov, O. A.; Izmaylov, A. F.; Scuseria, G. E. Influence of the exchange screening parameter on the performance of screened hybrid functionals. *J. Chem. Phys.* **2006**, *125*, 224106.
(40) May, M. M.; Supplie, O.; Hóhn, C.; van de Krol, R.; Lewerenz, H.-J.; Hannappel, T. The interface of GaP(100) and H_2O studied by photoemission and reflection anisotropy spectroscopy. *New J. Phys.* **2013**, *15*, 103003.
(41) Dues, C.; Schmidt, W. G.; Sanna, S. Water Splitting Reaction at Polar Lithium Niobate Surfaces. *ACS Omega* **2019**, *4*, 3850−3859.

https://doi.org/10.1021/acsomega.2c00948
ACS Omega 2022, 7, 19355−19364